

Article

Porous vs. Nanotubular Anodic TiO₂: Does the Morphology Really Matters for the Photodegradation of Caffeine?

Muhammad Bilal Hanif ^{1,†}, Marcel Sihor ^{2,†}, Viktoriia Liapun ^{1,3}, Hryhorii Makarov ⁴, Olivier Monfort ¹ and Martin Motola ^{1,*}

¹ Department of Inorganic Chemistry, Faculty of Natural Sciences, Comenius University in Bratislava, Ilkovicova 6, Mlynska Dolina, 842 15 Bratislava, Slovakia; hanif1@uniba.sk (M.B.H.); liapun1@uniba.sk (V.L.); monfort1@uniba.sk (O.M.)

² Institute of Environmental Technology, CEET, VSB-Technical University of Ostrava, 17, listopadu 15/2172, 70800 Ostrava-Poruba, Czech Republic; marcel.sihor@vsb.cz

³ Department of Environmental Ecology and Landscape Management, Faculty of Natural Sciences, Comenius University in Bratislava, Ilkovicova 6, Mlynska Dolina, 842 15 Bratislava, Slovakia

⁴ Department of Experimental Physics, Mathematics, and Informatics, Comenius University in Bratislava, 842 48 Bratislava, Slovakia; makarov1@uniba.sk

* Correspondence: martin.motola@uniba.sk; Tel.: +421-2-9014-9374

† These authors contributed equally to this work.

Abstract: Herein, the preparation of nanotubular and porous TiO₂ structures (TNS) is presented for photocatalytic applications. Different TNS were prepared in three different types of glycerol- and ethylene glycol-based electrolytes on a large area (approx. 20 cm²) via anodization using different conditions (applied potential, fluoride concentration). Morphology, structure, and optical properties of TNS were characterized by Scanning Electron Microscopy (SEM), X-ray Diffractometry (XRD), and Diffuse Reflectance Spectroscopy (DRS), respectively. All TNS possess optical band-gap energy (E_{BG}) in the range from 3.1 eV to 3.2 eV. Photocatalytic degradation of caffeine was conducted to evaluate the efficiency of TNS. Overall, nanotubular TiO₂ possessed enhanced degradation efficiencies (up to 50% degradation) compared to those of porous TiO₂ (up to 30% degradation). This is due to the unique properties of nanotubular TiO₂, e.g., improved incident light utilization. As the anodization of large areas is, nowadays, becoming a trend, we show that both nanotubular and porous TiO₂ are promising for their use in photocatalysis and could be potentially applicable in photoreactors for wastewater treatment. We believe this present work can be the foundation for future development of efficient TiO₂ nanostructures for industrial applications.

Keywords: nanotubular TiO₂; porous TiO₂; anodization; large area; photocatalysis; caffeine



Citation: Hanif, M.B.; Sihor, M.; Liapun, V.; Makarov, H.; Monfort, O.; Motola, M. Porous vs. Nanotubular Anodic TiO₂: Does the Morphology Really Matters for the Photodegradation of Caffeine? *Coatings* **2022**, *12*, 1002. <https://doi.org/10.3390/coatings12071002>

Academic Editor: Alexandru Enesca

Received: 29 June 2022

Accepted: 15 July 2022

Published: 16 July 2022

Publisher's Note: MDPI stays neutral with regard to jurisdictional claims in published maps and institutional affiliations.



Copyright: © 2022 by the authors. Licensee MDPI, Basel, Switzerland. This article is an open access article distributed under the terms and conditions of the Creative Commons Attribution (CC BY) license (<https://creativecommons.org/licenses/by/4.0/>).

1. Introduction

Electrochemical anodic oxidation (anodization) will soon celebrate 100 years since it was first patented in 1923 by Bengough and Stuart for its use on an industrial scale [1]. In general, the purpose of anodization is to passivate the surface of a material (primarily metals). Thus, the surface of the material develops a protective layer (in the form of oxide), which protects it against future corrosion. Pioneering works were conducted in 1984 [2] and 1995 [3] that allowed the preparation of not only a protective layer, but a unique nanotubular structure of TiO₂ and Al₂O₃, respectively, for several applications in several fields including energy, environment, medicine, and technology. Ever since the anodization of metals gained significant attention from the scientific community, thousands of papers have been related to anodization [4–6].

In particular, anodic TiO₂ nanotube layers [7] with unique properties of a 1D material are promising for photocatalysis [8], hydrogen production [9], DSSCs [10], or biomedical applications [11]. This is due to [7]: (i) high specific surface area and enhanced light

absorption due to the materials' 1D structure, (ii) a vertical transport of the photogenerated charge carriers (electron/holes), and (iii) tunable dimensions of the nanotubes, in particular, their length and diameter. In the last decade, organic-based electrolytes (e.g., glycerol and ethylene glycol) are the most popular for the preparation of TiO₂ nanotube layers via anodization [7]. Indeed, in such electrolytes, a high-aspect ratio and smooth nanotubes are prone to form [12]. Nevertheless, there are still major challenges in the synthesis and application of TiO₂ nanotube layers in industry. Indeed, layers of several cm² are necessary and this relates to specific preparation challenges, i.e., when a potential is applied to areas of several cm², the absolute current flowing between the two electrodes is much higher compared to that of smaller areas (most of the published articles report a laboratory scale of 1 cm² area) [7]. The flowing high current leads to an increase in the electrolyte temperature and subsequently a dielectric breakdown will occur [13]. To this day, only a few reports deal with the preparation of TiO₂ nanotube layers on areas >10 cm² [9,13–20]. A field-assisted dissolution of titanium supported by fluoride ions is responsible for the formation of a nanotubular structure [7]. Thus, by using optimized anodization conditions, TiO₂ nanotube layers are formed. Nevertheless, there is a thin line between the formation of a nanotubular and a porous structure of TiO₂. The potential/current induced dissolution of the formed TiO₂ in the presence of fluoride ions via [TiF₆]²⁻ is well known to the scientific community [21,22]. In case that the dissolution rate is higher than the formation rate, a rather porous structure is formed instead of a nanotubular one. Such a porous TiO₂ is often overlooked in the literature, as it is considered an unsuccessful preparation of TiO₂ nanotube layers. However, this formed porous TiO₂ possesses a high specific surface area and a sufficient number of active sites necessary for, e.g., photocatalysis similarly to nanotubular TiO₂. In our recent work [9], we reported that both nanotubular and porous anodic TiO₂ nanostructures (TNS) possess efficient properties in the photocatalytic degradation of caffeine and hydrogen production. Therefore, we aim this work as a follow-up to our recent paper. Here, we focus solely on the degradation of caffeine (i.e., liquid phase photocatalysis) by using different types of anodic nanotubular and porous TNS prepared via anodization on a large area to gain knowledge about these two, although, different but in many ways similar materials. We believe that both nanotubular and porous anodic TNS are promising for the application in photo-induced processes including photocatalysis.

In the present work, TNS on a large area (approx. 20 cm²) were prepared via anodization in different organic-based electrolytes (i.e., glycerol and ethylene glycol) containing fluoride ions. Scanning Electron Microscopy (SEM), X-ray Diffractometry (XRD), and Diffuse Reflectance Spectroscopy (DRS) was conducted to ensure the morphology, crystal structure, and optical properties of the prepared TNS, respectively. Caffeine was employed as a model organic pollutant to evaluate the photocatalytic activity of the prepared TNS. The present work critically discusses the pros and cons of nanotubular and porous anodic TiO₂ for application in liquid-phase photocatalysis. It is worthy to note that herein, we do not aim for 100% pollutant degradation, but rather for a fundamental understanding of different TNS for future development in photocatalysis.

2. Materials and Methods

2.1. Synthesis of TNS

Titanium foil (Sigma-Aldrich, Darmstadt, Germany, 99.7% purity, 0.127 mm thickness, 20 cm² area) was used as a starting substrate for the formation of TNS. According to our previous work [9], a circle of 5 cm in diameter was drawn on the square titanium foil and cut out into three corners to make a drop-like shape which was used as a working electrode (titanium foil of 5 × 2 cm² was used as a counter electrode). One corner of the electrode was utilized as a handle to fasten the electrode. The distance between the electrodes was kept at 1.6 cm. Anodization was conducted using potential from 20 V to 80 V (20 V step) for 100 min in glycerol- (Central-Chem, Bratislava, Slovakia) and ethylene glycol-based (Central-Chem, Bratislava, Slovakia) electrolytes. To avoid overheating of the electrolyte,

cooling with an ice bath was conducted to possess a constant temperature of 8 °C during anodization. Three different types of electrolytes based on either glycerol or ethylene glycol were used for the synthesis of TNS according to our previous works [9,23]. We also used three optimized electrolyte compositions, which our group often uses [24–30]. Moreover, we varied the concentration of fluoride ions by decreasing it to 75% and 50% of the initial amount (100%), respectively, for each electrolyte. Thus, we obtained altogether 9 different electrolytes and the electrolyte compositions along with the materials' abbreviations and the used anodization conditions are summarized in Table 1. By these efforts, both nanotubular and porous TiO₂ structures were obtained as required for the purpose of this study. After synthesis, TNS were immersed in isopropanol to remove the electrolyte leftovers from the surface and subsequently annealed in a muffle oven at 400 °C in air (2.21 °C/min heating rate). Afterward, TNS were cooled down inside the oven to room temperature.

Table 1. Summary: electrolyte abbreviation, composition, and applied potential.

Electrolyte	Electrolyte Composition	Electrolyte	Electrolyte Composition	Electrolyte	Electrolyte Composition	Applied Potential (V)
EL1 _{100%}	2 g NH ₄ F; 100 mL glycerol; 100 mL H ₂ O	EL2 _{100%}	1.3 g NH ₄ F; 197 mL ethylene glycol; 3 mL H ₂ O	EL3 _{100%}	1.1045 g NH ₄ F; 180 mL ethylene glycol; 20 mL H ₂ O	20
						40
						60
						80
EL1 _{75%}	1.5 g NH ₄ F; 100 mL glycerol; 100 mL H ₂ O	EL2 _{75%}	0.975 g NH ₄ F; 197 mL ethylene glycol; 3 mL H ₂ O	EL3 _{75%}	0.83 g NH ₄ F; 180 mL ethylene glycol; 20 mL H ₂ O	20
						40
						60
						80
EL1 _{50%}	1 g NH ₄ F; 100 mL glycerol; 100 mL H ₂ O	EL2 _{50%}	0.65 g NH ₄ F; 197 mL ethylene glycol; 3 mL H ₂ O	EL3 _{50%}	0.55 g NH ₄ F; 180 mL ethylene glycol; 20 mL H ₂ O	20
						40
						60
						80

2.2. Characterization and Photocatalytic Activity of TNS

Morphology and structure of the TNS layers was studied using Scanning Electron Microscopy (SEM, Lyra 3 Tescan, Tescan, Brno, Czech Republic, at 10 kV) equipped with Energy-Dispersive X-ray Spectroscopy (EDS) and X-ray Diffractometer (20°–60° 2 Theta; XRD, PANalytical Cu K α radiation, $\lambda = 1.5418 \text{ \AA}$, Malvern-Panalytical, Malvern, United Kingdom), respectively. Optical properties were studied via Diffuse Reflectance Spectroscopy in the wavelength range from 200 nm to 800 nm (DRS, Shimadzu UV-2600, Shimadzu, Kyoto, Japan) equipped with an integrating sphere 2600 Plus.

Photocatalytic degradation of caffeine (CAF, Reagent Plus, Sigma-Aldrich, Darmstadt, Germany) aqueous solution (10 ppm, 50 mL) was evaluated in a home-made photoreactor, which consisted of a circular glass dish with a diameter of 8 cm. A sample carrier was placed at the bottom of the glass dish. Prior to the photocatalytic measurements, the whole assembly (along with TNS) was placed in the dark for 20 min to achieve the adsorption/desorption equilibrium. Afterwards, an 8W Hg lamp (Ultra-Violet Products Inc. UVP, Upland, CA, USA, $\lambda_{\text{max}} = 365 \text{ nm}$) was used as the radiation source. The degradation of CAF was monitored for 3 h at 20 min intervals. The solution was withdrawn (0.5 mL) with a micropipette and mixed with 0.5 mL of distilled water. The concentration of CAF was determined by UV-VIS spectrophotometer (Jasco V530, Kyoto, Japan), according to our previous work [9]. To confirm the good stability of all TNSs, the photocatalytic activity measurements were repeated 3 times for each sample, and the differences in the overall photocatalytic performance did not exceed $\pm 5\%$.

3. Results and Discussion

Anodization of a 20 cm² area Ti was conducted using fluoride-containing glycerol- and ethylene glycol-based electrolytes to obtain the herein-presented materials. The an-

odization conditions that we used led to the formation of both nanotubular and porous TiO₂ structures. Therefore, to avoid any confusion, we abbreviated the prepared materials as TNS (TiO₂ nanostructures).

Representative SEM images of TNS prepared in EL1, EL2 and EL33 with different concentrations of fluoride ions (according to Table 1) at 60 V are shown in Figure 1. Using similar conditions (voltage and anodization time), both nanotubular and porous structures were formed, depending primarily on the electrolyte composition. We conducted the SEM analysis on all the prepared TNS according to Table 1; however, we did not include all the SEM images in the manuscript (*not to overload the manuscript with plenty of SEM images*). The surface of each prepared TNS possess similar surface morphology as seen in Figure 1. Nevertheless, we summarized the morphological features (tube/pore diameter and thickness of the layer) of each TNS in Table 2, i.e., TNS prepared in different electrolytes (glycerol- or ethylene glycol-based ones), with different concentrations of fluoride ions (according to Table 1), at different applied potentials (from 20 V to 80 V). In general, electrolyte composition and applied conditions during anodization are crucial factors that affect the final morphology of TNS. Fluoride ions present in electrolytes act as etching agents and are directly responsible for the formation of either nanotubular or porous structures [21,22,31–33]. Generally, when the dissolution rate is higher than the formation rate, a rather porous structure is formed instead of a nanotubular one [34]. Thus, the mechanical stability of the formed nanotubular structure is disturbed, and as a result, a collapse of the tubes' mouth is observed. Nevertheless, both nanotubular and porous structures possess good adhesion to the underlying Ti substrate, i.e., the formed layers do not peel off the substrate after bending. Moreover, both structures are efficient in applications such as photocatalysis and hydrogen production [9].

Table 2. Morphological features of the prepared TNS in different electrolytes.

Electrolyte	Applied Potential (V)	Morphological Features		
		Structure Type	Pore Diameter (nm)	Layer Thickness (μm)
EL1 _{100%}	20	Nanotubular	30–60	3–4
	40	Nanotubular	40–70	6–8
	60	Porous	50–100	7–9
	80	Porous	50–100	9–12
EL1 _{75%}	20	Nanotubular	20–40	6–8
	40	Nanotubular	50–80	6–8
	60	Porous	50–100	6–8
	80	Porous	50–100	8–10
EL1 _{50%}	20	Nanotubular	10–20	2–4
	40	Nanotubular	30–50	2–4
	60	Porous	50–100	4–5
	80	Porous	50–100	5–6
EL2 _{100%}	20	Porous	10–30	7–8
	40	Nanotubular	20–50	12–17
	60	Nanotubular	30–40	13–17
	80	Nanotubular	40–60	14–17
EL2 _{75%}	20	Porous	10–20	4–6
	40	Nanotubular	30–50	4–8
	60	Nanotubular	40–50	8–9
	80	Nanotubular	40–50	9–12
EL2 _{50%}	20	Porous	5–20	1–2
	40	Nanotubular	20–40	1–2
	60	Nanotubular	30–40	2–3
	80	Nanotubular	30–40	3–4

Table 2. Cont.

Electrolyte	Applied Potential (V)	Morphological Features		
		Structure Type	Pore Diameter (nm)	Layer Thickness (μm)
EL3 _{100%}	20	Nanotubular	30–50	3–5
	40	Porous	30–70	3–5
	60	Porous	50–80	4–7
	80	Porous	60–80	6–9
EL3 _{75%}	20	Nanotubular	20–40	2–3
	40	Porous	40–70	2–3
	60	Porous	50–80	4–6
	80	Porous	60–80	4–8
EL3 _{50%}	20	Nanotubular	10–20	1–2
	40	Porous	10–30	1–3
	60	Porous	50–80	2–5
	80	Porous	50–90	4–7

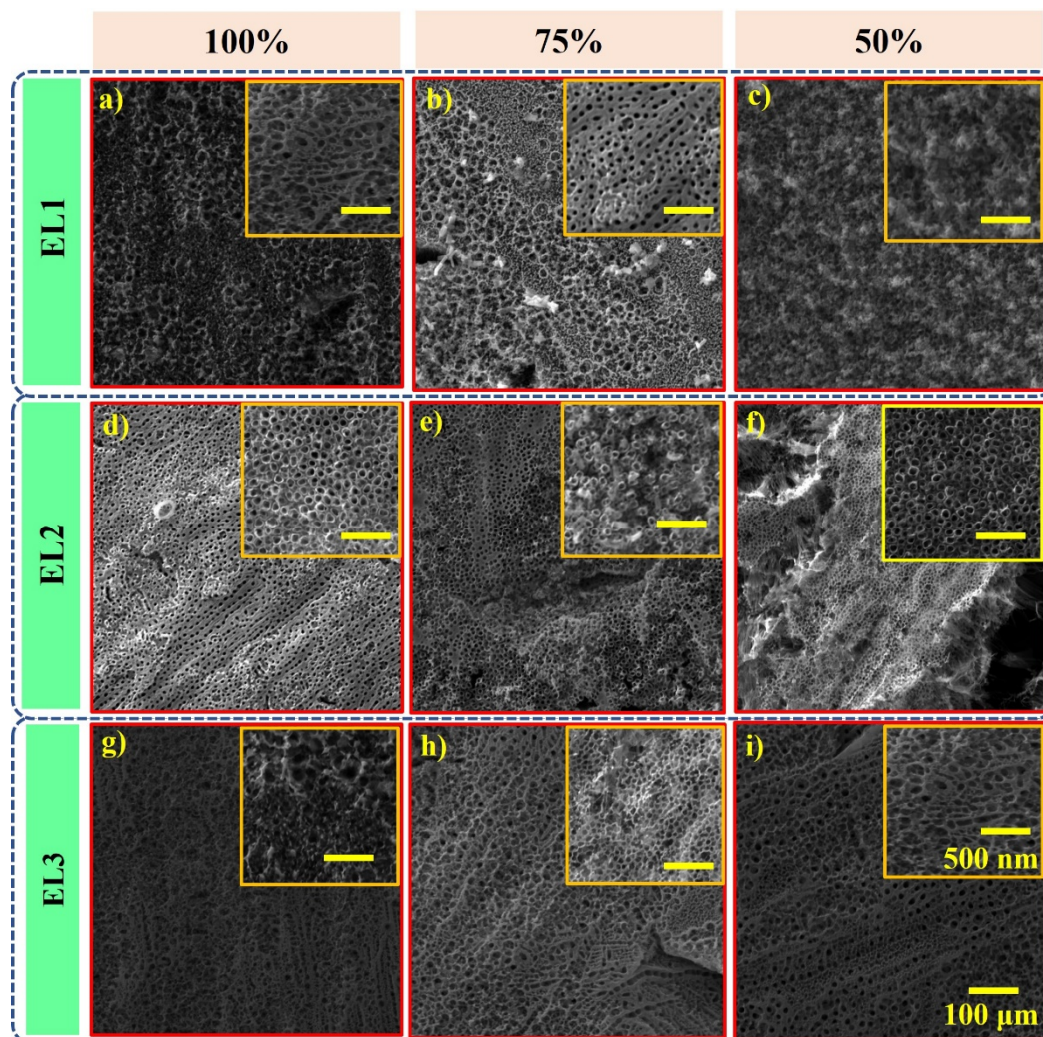


Figure 1. Representative SEM images of TNS prepared in different electrolytes (according to Table 1) at 60 V: (a–c) EL1_{100%}, EL1_{75%}, and EL1_{50%}, respectively, (d–f) EL2_{100%}, EL2_{75%}, and EL2_{50%}, respectively, and (g–i) EL3_{100%}, EL3_{75%}, and EL3_{50%}, respectively.

Several trends were observed from the obtained data summarized in Table 1 and are as follows: In all types of electrolytes, the pore diameter and thickness of the nanotubular

or porous TiO₂ layer increased with the increased potential. This is in accordance with the plethora of reports on the effect of anodization conditions on the morphology of the layers [7,35–37]. In general, at higher potentials (i.e., 60 V and 80 V), rather a porous structure is formed instead of a nanotubular one. Indeed, the etching rate is higher at increased potentials; thus, a porous structure formation is present. At lower potentials (i.e., 20 V and 40 V) a nanotubular structure is prone to form. Nevertheless, in the case of EL2, the porous structure was observed at 20 V, and nanotubular structures were formed at 40 V, 60 V, and 80 V. This is due to the low content of distilled water in the electrolyte (3 mL); thus, higher potentials are required for nanotubular structure to be obtained [7]. Indeed, the viscosity of the electrolyte that contains 197 mL of ethylene glycol and 3 mL of distilled water inhibits the migration of fluoride ions present in the electrolyte during anodization.

Figure 2 shows XRD patterns of annealed TNS; XRD was performed on all the TNS (a total of 36 samples), but the applied potential during anodization (20 V–80 V) and electrolyte composition has no impact on the phase composition of the material after annealing, and all the TNS possess similar phase composition. Therefore, we included representative XRD patterns for each electrolyte type (according to Table 1) prepared at 60 V. In all TNS, two different phases were identified, i.e., tetragonal anatase TiO₂ (P4₂/mm; ICDD 01-086-1157) [38,39] and hexagonal metallic Ti (P6₃/mmc; ICDD 00-044-1294) [23]. The visible diffractions of metallic Ti stem from the underlying Ti substrate and are visible due to the penetration of X-rays. Nevertheless, the prepared nanotubular and porous TiO₂ structures consist solely of anatase TiO₂. The XRD patterns show typical diffractions of anodically prepared TiO₂ layers [9,23].

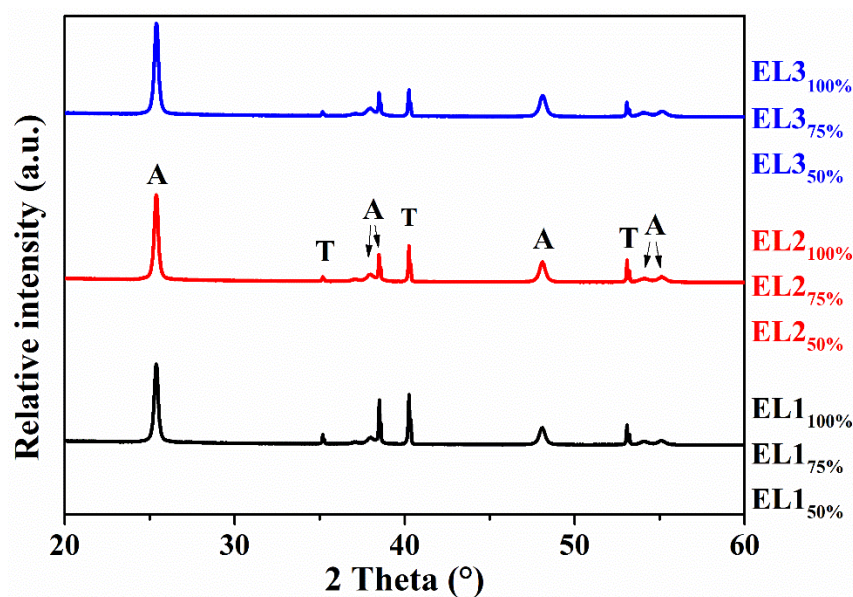


Figure 2. XRD patterns of TNS prepared in different electrolytes (according to Table 1) at 60 V. A—anatase; T—titanium.

UV-VIS DRS spectra and the corresponding Kubelka–Munk curves were recorded to determine the reflectance and the indirect optical band gap energy (E_{BG}) of TNS (Figure 3). Although DRS measurements were performed on all TNS, we show representative spectra of TNS prepared at 60 V (similarly to SEM in Figure 1 and XRD in Figure 2). All TNS (36 different ones) possess similar optical properties with E_{BG} in the energy range from 3.1 eV to 3.2 eV. The obtained values of the indirect E_{BG} are in good agreement with previous reports on TiO₂ materials composed solely of the anatase phase [40–43]. Indeed, the appeared reflectance edge at ~400 nm is attributed to the anatase phase with E_{BG} ~3.2 eV [44], and no substantial differences were observed in the different TNS. Both nanotubular and porous structures contain solely anatase TiO₂, thus their E_{BG} are similar.

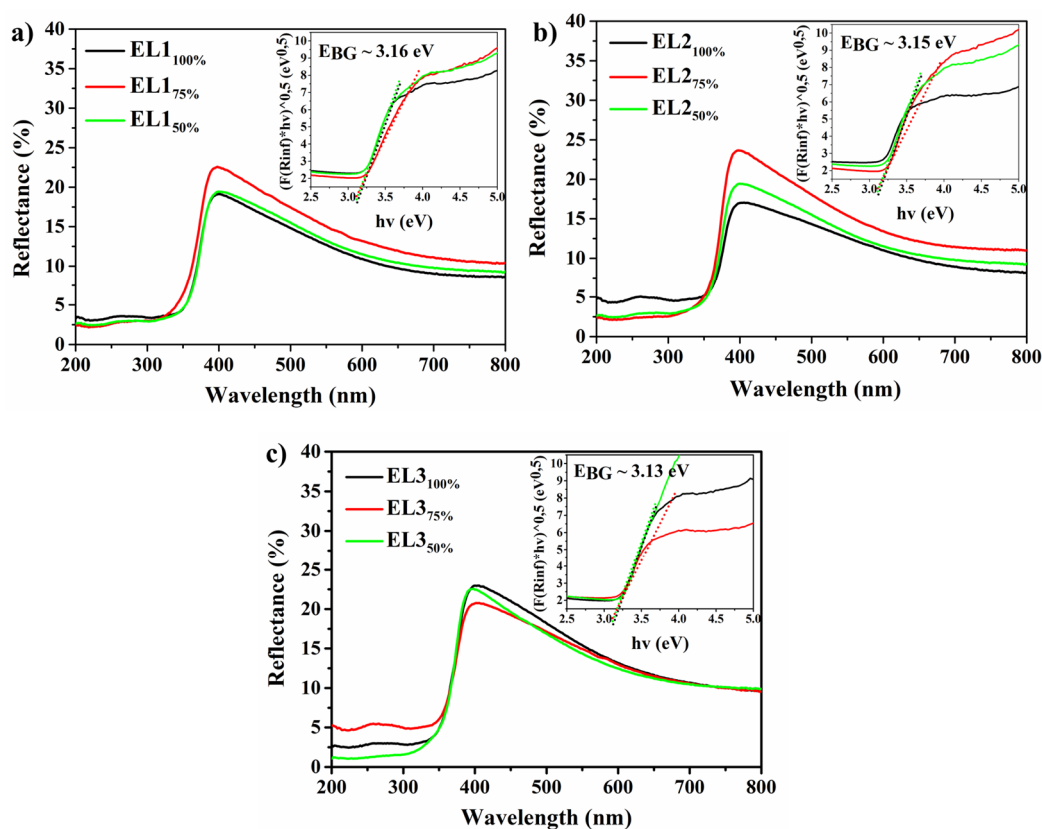


Figure 3. UV-VIS DRS spectra and the corresponding Kubelka–Munk curves (as insets) of TNS prepared in different electrolytes (according to Table 1) at 60 V: (a) EL1_{50%}–EL1_{100%}, (b) EL2_{50%}–EL2_{100%}, and (c) EL3_{50%}–EL3_{100%}.

Photocatalytic degradation of caffeine (CAF) was explored under UVA light irradiation ($\lambda_{\max} = 365$ nm) on all TNS, and the results are summarized in Figure 4, along with the illustration of the photoreactor that was used. Photocatalytic degradation of CAF follows the first-order reaction typical for TiO₂ photocatalysts and an organic pollutant [45]. Although the degradation rates were calculated, we decided to add the conversion efficiency of CAF in % for an easier and more understandable interpretation of the results (*to avoid 36 different rate constants that would confuse the reader*). The conversion efficiency was calculated directly from the degradation extents after 3 h, i.e., from the initial and final concentration of CAF. Overall, the most efficient CAF degradation was obtained using nanotubular structures. Indeed, the unique properties of the nanotubular TiO₂ structures, such as improved charge carrier transport along the nanotube walls and overall enhanced incident light utilization is responsible for this outcome. The most efficient TNS (EL2_{100%} at prepared 40 V) degraded approx. 50% of the pollutant. A clear trend appeared wherein by decreasing the amount of fluoride ions during anodization, the photocatalytic degradation efficiency decreased. Indeed, fluoride ions are responsible for the formation of nanotubular and porous TiO₂ structures; thus, by lowering the total amount of fluorides, the etching rate during anodization is low. As a result of the low content of fluorides, thinner layers are obtained during anodization in EL1-3_{50%} as seen in Table 2 (*with a maximum thickness of approx. 5 μ m*). With the increasing of the fluoride content in the electrolytes (EL1-3_{75%}–100%), the thickness substantially increased and reached approx. 17 μ m in EL2_{100%}. Moreover, the pore diameter is another crucial factor that directly affects the specific surface area. Herein, Brunauer–Emmett–Telle (BET) theory [46] is not applicable in the case of TNS, as it is challenging to measure BET on our kind of samples, i.e., to remove the layers from the underlying substrate and proceed with the BET measurements. Nevertheless, the obtained SEM data (Figure 1) show clear differences in the pore diameter; thus, it indirectly confirms a high surface area of the material, in general. As the degradation

of CAF proceeds at the TNS/CAF interface, surface area (or porosity) is a crucial factor. The interplay of morphology (SEM, Figure 1), structure (XRD, Figure 2), and optical properties (DRS and Kubelka–Munk plots, Figure 3) are in favor of the photocatalytic efficiency of the herein-presented TNS prepared in glycerol- and ethylene glycol-based electrolytes with higher concentration of fluoride ions. The porous TiO₂ structures showed approx. 2 times lower degradation efficiencies. This is due collapse/distortion of the nanotubular structure during anodization by the applied conditions. The pores are denser, thus providing fewer active sites for CAF to be adsorbed and subsequently degraded. Nevertheless, a satisfactory degradation efficiency of CAF (approx. 30%) was obtained by using porous TiO₂ (EL3_{100%} prepared at 60 V). All in all, both nanotubular and porous TiO₂ structures prepared via anodization are promising for application in photoreactors for wastewater treatment. Nevertheless, there are still major challenges of synthesis such nanostructures on large area, and such synthesis is necessary for industrial applications of these nanomaterials. At last, Table 3 shows the comparison of our TNS with reports on anodic TiO₂ based nanostructures for caffeine photocatalytic degradation.

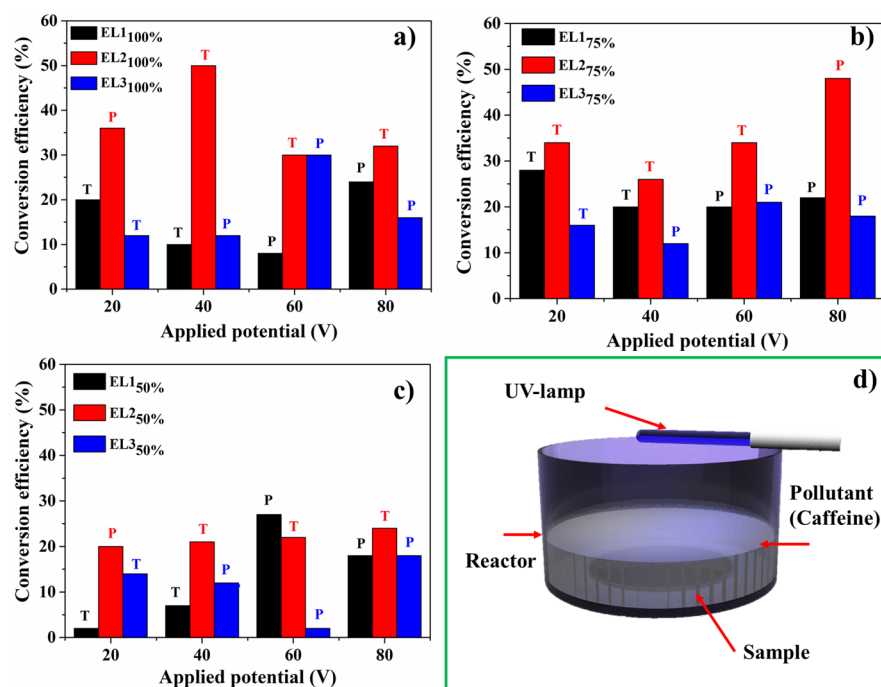


Figure 4. Photocatalytic degradation of caffeine using TNS prepared in different electrolytes (according to Table 1): (a) EL1-3_{100%}, (b) EL1-3_{75%}, (c) EL1-3_{50%}, and (d) illustration of the photocatalytic reactor. T—nanotubular; P—porous.

Table 3. The comparison of anodic TiO₂ based nanostructure for caffeine photocatalytic degradation. Anodization condition, target pollutant (and its concentration), rate constant, and time duration were taken from the literature.

Material	Anodization Conditions	Caffeine Concentration	Rate constant (k)/ Conversion Efficiency (%)	Time (min)	Ref
TiO ₂	Glycol electrolyte with 0.3 wt % NH ₄ F and 2 vol % DI-H ₂ O (60 V for 6 h)	50 mg L ⁻¹	44%	180	[47]
TiO ₂	2g NH ₄ F + 100 mL DI-H ₂ O in glycerol-based electrolyte (20 V for 100 min).	20 ppm	0.0069 min ⁻¹	120	[9]
V- TiO ₂	NH ₄ F (1.3 g) in EG (197 mL) and DI-H ₂ O (3 mL).	20 ppm	46%	120	[48]
TiO ₂	98% ethylene glycol, 2% DI-H ₂ O and 0.3 wt % NH ₄ F.	15 mg L ⁻¹	51%	240	[49]
TiO ₂	EG and a solution of 0.3 wt % NH ₄ F in 2 vol % DI-H ₂ O (60 V for 3 h)	10 ppm	2.12 ± 0.13 × 10 ⁻² min ⁻¹	180 min	[50]
EL2 ₁₀₀ %	1.3 g NH ₄ F; 197 mL EG; 3 mL H ₂ O (40 V for 100 min)	10 ppm	50%	180 min	This study
EL2 ₇₅ %	0.975 g NH ₄ F; 197 mL EG; 3 mL H ₂ O (80 V for 100 min)	10 ppm	50%	180 min	This study

4. Conclusions

Anodization of an approx. 20 cm² Ti area was conducted to prepare nanotubular and porous TiO₂ structures for comparison in the photocatalytic degradation of caffeine under UVA. A variety of conditions were conducted to obtain a total of 36 different TNS: (i) three different electrolytes based on glycerol and ethylene glycol, (ii) three different concentrations of fluoride ions in each type of electrolyte, and (iii) different applied potentials from 20 V to 80 V for each type of electrolyte. Depending on the different conditions, nanotubular and porous TiO₂ structures were formed with thickness up to 17 µm and pore diameter up to 100 nm, and subsequently annealed at 400 °C to obtain crystalline anatase TiO₂. All TNS possess E_{BC} in the range from 3.1 eV to 3.2 eV. Overall, both nanotubular and porous TNS lead to efficient degradation extents of caffeine after 3 h, although nanotubular TNS showed enhanced photocatalytic activity (reaching degradation up to 50%) compared to that of porous TNS. Indeed, the unique properties of 1D nanotubular structures are responsible for the improved photocatalytic activity. The degradation efficiency of both nanostructures is due to their high surface area associated with a sufficient number of active sites for caffeine to adsorb on the surface of TNS and subsequently degrade the pollutant. As the anodization of large areas is, nowadays, becoming a trend, we show that both nanotubular and porous TiO₂ are promising for their use in photocatalysis and could, potentially, be applicable in photoreactors for wastewater treatment. We believe this present work can be the foundation for future development of efficient TiO₂ nanostructures for industrial applications.

Author Contributions: Conceptualization, M.M.; methodology, M.S., M.B.H., V.L., O.M. and M.M.; software, M.S. and M.B.H.; validation, M.S., M.B.H. and M.M.; formal analysis, M.S., H.M., M.B.H. and V.L.; investigation M.S., M.B.H. and H.M.; resources, M.M.; data curation, M.B.H.; writing—original draft preparation, M.S., M.B.H., O.M. and M.M.; writing—review and editing, M.S., M.B.H., V.L., O.M. and M.M.; visualization, M.S. and M.B.H.; supervision, M.M.; project administration, M.M.; funding acquisition, M.S., O.M., M.B.H. and M.M. All authors have read and agreed to the published version of the manuscript.

Funding: This work was co-financed by (i) Slovak Research and Development Agency (APVV): contracts No. APVV-21-0039 and No. APVV-21-0053, (ii) Scientific Grant Agency of the Slovak Ministry of Education, Sciences, Research and Sport (VEGA): project No. 1/0062/22, (iii) Grant of the Comenius University Bratislava for Young Scientists (UK/3/2022), (iv) the ESF in “Science without borders 2.0” project, reg. nr. CZ.02.2.69/0.0/0.0/18_053/0016985 within the Operational Programme Research, Development and Education, and (v) ERDF “Institute of Environmental Technology-Excellent Research” (No. CZ.02.1.01/0.0/0.0/16_019/0000853). This work has also been partially supported by the project USCCCOR (ŽoNFP:NFP313020BUZ3), co-financed by the European Regional Development Fund within the Operational Programme Integrated Infrastructure.

Institutional Review Board Statement: Not applicable.

Informed Consent Statement: Not applicable.

Data Availability Statement: The data presented in this study are available on request from the corresponding author.

Conflicts of Interest: The authors declare no conflict of interest.

References

1. Bengough, G.D.; Stuart, J.M. Improved Process of Protecting Surfaces of Aluminium of Aluminium Alloys. *UK Pat.* **1923**, 223, 36.
2. Assefpour-Dezfuly, M.; Vlachos, C.; Andrews, E.H. Oxide Morphology and Adhesive Bonding on Titanium Surfaces. *J. Mater. Sci.* **1984**, *19*, 3626–3639. [[CrossRef](#)]
3. Masuda, H.; Fukuda, K. Ordered Metal Nanohole Arrays Made by a Two-Step Replication of Honeycomb Structures of Anodic Alumina. *Science* **1995**, *268*, 1466–1468. [[CrossRef](#)] [[PubMed](#)]
4. El-Said Shehata, O.; Abdel-karim, A.M.; Abdel Fatah, A.H. New Trends in Anodizing and Electrolytic Coloring of Metals. *Egypt. J. Chem.* **2022**, *65*, 229–241. [[CrossRef](#)]
5. David, T.M.; Dev, P.R.; Wilson, P.; Sagayaraj, P.; Mathews, T. A Critical Review on the Variations in Anodization Parameters toward Microstructural Formation of TiO₂ Nanotubes. *Electrochem. Sci. Adv.* **2021**, e202100083. [[CrossRef](#)]
6. Minagar, S.; Berndt, C.C.; Wang, J.; Ivanova, E.; Wen, C. A Review of the Application of Anodization for the Fabrication of Nanotubes on Metal Implant Surfaces. *Acta Biomater.* **2012**, *8*, 2875–2888. [[CrossRef](#)]
7. Lee, K.; Mazare, A.; Schmuki, P. One-Dimensional Titanium Dioxide Nanomaterials: Nanotubes. *Chem. Rev.* **2014**, *114*, 9385–9454. [[CrossRef](#)]
8. Macak, J.M.; Zlamal, M.; Krysa, J.; Schmuki, P. Self-Organized TiO₂ Nanotube Layers as Highly Efficient Photocatalysts. *Small* **2007**, *3*, 300–304. [[CrossRef](#)]
9. Šihor, M.; Hanif, M.B.; Thirunavukkarasu, G.K.; Liapun, V.; Edelmannova, M.F.; Roch, T.; Satrapinsky, L.; Plecenik, T.; Rauf, S.; Hensel, K.; et al. Anodization of Large Area Ti: Versatile Material for Caffeine Photodegradation and Hydrogen Production. *Catal. Sci. Technol.* **2022**. [[CrossRef](#)]
10. O'Regan, B.; Grätzel, M. A Low-Cost, High-Efficiency Solar Cell Based on Dye-Sensitized Colloidal TiO₂ Films. *Nature* **1991**, *353*, 737–740. [[CrossRef](#)]
11. Motola, M.; Capek, J.; Zazpe, R.; Bacova, J.; Hromádka, L.; Bruckova, L.; Ng, S.; Handl, J.; Spatz, Z.; Knotek, P.; et al. Thin TiO₂ Coatings by ALD Enhance the Cell Growth on TiO₂ Nanotubular and Flat Substrates. *ACS Appl. Bio Mater.* **2020**, *3*, 6447–6456. [[CrossRef](#)] [[PubMed](#)]
12. Macak, J.M.; Tsuchiya, H.; Taveira, L.; Aldabergerova, S.; Schmuki, P. Smooth Anodic TiO₂ Nanotubes. *Angew. Chemie Int. Ed.* **2005**, *44*, 7463–7465. [[CrossRef](#)] [[PubMed](#)]
13. Sopha, H.; Baudys, M.; Krbal, M.; Zazpe, R.; Prikryl, J.; Krysa, J.; Macak, J.M. Scaling up Anodic TiO₂ Nanotube Layers for Gas Phase Photocatalysis. *Electrochem. Commun.* **2018**, *97*, 91–95. [[CrossRef](#)]
14. Motola, M.; Satrapinsky, L.; Roch, T.; Šubrt, J.; Kupčík, J.; Klementová, M.; Jakubičková, M.; Peterka, F.; Plesch, G. Anatase TiO₂ nanotube Arrays and Titania Films on Titanium Mesh for Photocatalytic NO_x removal and Water Cleaning. *Catal. Today* **2017**, *287*, 59–64. [[CrossRef](#)]
15. Mena, E.; Martín de Vidales, M.J.; Mesones, S.; Marugán, J. Influence of Anodization Mode on the Morphology and Photocatalytic Activity of TiO₂-NTs Array Large Size Electrodes. *Catal. Today* **2018**, *313*, 33–39. [[CrossRef](#)]
16. Szkoda, M.; Trzciński, K.; Zarach, Z.; Roda, D.; Łapiński, M.; Nowak, A.P. Scaling Up the Process of Titanium Dioxide Nanotube Synthesis and Its Effect on Photoelectrochemical Properties. *Materials* **2021**, *14*, 5686. [[CrossRef](#)]
17. Kim, H.-I.; Kim, D.; Kim, W.; Ha, Y.-C.; Sim, S.-J.; Kim, S.; Choi, W. Anodic TiO₂ Nanotube Layer Directly Formed on the Inner Surface of Ti Pipe for a Tubular Photocatalytic Reactor. *Appl. Catal. A Gen.* **2016**, *521*, 174–181. [[CrossRef](#)]
18. Xiang, C.; Sun, L.; Wang, Y.; Wang, G.; Zhao, X.; Zhang, S. Large-Scale, Uniform, and Superhydrophobic Titania Nanotubes at the Inner Surface of 1000 Mm Long Titanium Tubes. *J. Phys. Chem. C* **2017**, *121*, 15448–15455. [[CrossRef](#)]
19. Ghosh, J.P.; Achari, G.; Langford, C.H. Design and Evaluation of a UV LED Photocatalytic Reactor Using Anodized TiO₂ Nanotubes. *Water Environ. Res.* **2016**, *88*, 785–791. [[CrossRef](#)]

20. Franz, S.; Perego, D.; Marchese, O.; Bestetti, M. Photoelectrochemical Advanced Oxidation Processes on Nanostructured TiO₂ Catalysts: Decolorization of a Textile Azo-Dye. *J. Water Chem. Technol.* **2015**, *37*, 108–115. [[CrossRef](#)]
21. Zhang, W.; Liu, Y.; Guo, F.; Liu, J.; Yang, F. Kinetic Analysis of the Anodic Growth of TiO₂ Nanotubes: Effects of Voltage and Temperature. *J. Mater. Chem. C* **2019**, *7*, 14098–14108. [[CrossRef](#)]
22. Indira, K.; Mudali, U.K.; Nishimura, T.; Rajendran, N. A Review on TiO₂ Nanotubes: Influence of Anodization Parameters, Formation Mechanism, Properties, Corrosion Behavior, and Biomedical Applications. *J. Bio-Tribo-Corrosion* **2015**, *1*, 1–22. [[CrossRef](#)]
23. Motola, M.; Hromadko, L.; Prikryl, J.; Sopha, H.; Krbal, M.; Macak, J.M. Intrinsic Properties of High-Aspect Ratio Single- and Double-Wall Anodic TiO₂ Nanotube Layers Annealed at Different Temperatures. *Electrochim. Acta* **2020**, *352*, 136479. [[CrossRef](#)]
24. Michalkova, H.; Skubalova, Z.; Sopha, H.; Strmiska, V.; Tesarova, B.; Dostalova, S.; Svec, P.; Hromadko, L.; Motola, M.; Macak, J.M.; et al. Complex Cytotoxicity Mechanism of Bundles Formed from Self-Organised 1-D Anodic TiO₂ Nanotubes Layers. *J. Hazard. Mater.* **2020**, *388*, 122054. [[CrossRef](#)]
25. Motola, M.; Čaplovičová, M.; Krbal, M.; Sopha, H.; Thirunavukkarasu, G.K.; Gregor, M.; Plesch, G.; Macak, J.M. Ti³⁺ Doped Anodic Single-Wall TiO₂ Nanotubes as Highly Efficient Photocatalyst. *Electrochim. Acta* **2020**, *331*, 135374. [[CrossRef](#)]
26. Krbal, M.; Ng, S.; Motola, M.; Hromadko, L.; Dvorak, F.; Prokop, V.; Sopha, H.; Macak, J.M. Sulfur Treated 1D Anodic TiO₂ Nanotube Layers for Significant Photo- and Electroactivity Enhancement. *Appl. Mater. Today* **2019**, *17*, 104–111. [[CrossRef](#)]
27. Motola, M.; Sopha, H.; Krbal, M.; Hromádka, L.; Zmrhalová, Z.O.; Plesch, G.; Macak, J.M. Comparison of Photoelectrochemical Performance of Anodic Single- and Double-Walled TiO₂ nanotube Layers. *Electrochem. Commun.* **2018**, *97*, 1–5. [[CrossRef](#)]
28. Motola, M.; Baudys, M.; Zazpe, R.; Krbal, M.; Michalička, J.; Rodriguez-Pereira, J.; Pavliňák, D.; Prikryl, J.; Hromádka, L.; Sopha, H.; et al. 2D MoS₂ Nanosheets on 1D Anodic TiO₂ Nanotube Layers: An Efficient Co-Catalyst for Liquid and Gas Phase Photocatalysis. *Nanoscale* **2019**, *11*, 23126–23131. [[CrossRef](#)]
29. Motola, M.; Satrapinsky, L.; Čaplovičová, M.; Roch, T.; Gregor, M.; Grančič, B.; Greguš, J.; Čaplovič, L.; Plesch, G. Enhanced Photocatalytic Activity of Hydrogenated and Vanadium Doped TiO₂ nanotube Arrays Grown by Anodization of Sputtered Ti Layers. *Appl. Surf. Sci.* **2018**, *434*, 1257–1265. [[CrossRef](#)]
30. Motola, M.; Zazpe, R.; Hromadko, L.; Prikryl, J.; Címančová, V.; Rodriguez-Pereira, J.; Sopha, H.; Macak, J.M. Anodic TiO₂ Nanotube Walls Reconstructed: Inner Wall Replaced by ALD TiO₂ Coating. *Appl. Surf. Sci.* **2021**, *549*, 149306. [[CrossRef](#)]
31. Cha, G.; Schmuki, P.; Altomare, M. Free-Standing Membranes to Study the Optical Properties of Anodic TiO₂ Nanotube Layers. *Chem. Asian J.* **2016**, *11*, 789–797. [[CrossRef](#)] [[PubMed](#)]
32. Fraoucene, H.; Sugawati, V.A.; Hatem, D.; Belkaid, M.S.; Vacandio, F.; Eyraud, M.; Pasquinelli, M.; Djenizian, T. Optical and Electrochemical Properties of Self-Organized TiO₂ Nanotube Arrays from Anodized Ti-6Al-4V Alloy. *Front. Chem.* **2019**, *7*, 66. [[CrossRef](#)] [[PubMed](#)]
33. Pishkar, N.; Jedi-soltanabadi, Z.; Ghoranneviss, M. Reduction in the Band Gap of Anodic TiO₂ Nanotube Arrays by H₂ Plasma Treatment. *Results Phys.* **2018**, *10*, 466–468. [[CrossRef](#)]
34. Varghese, O.K.; Gong, D.; Paulose, M.; Grimes, C.A.; Dickey, E.C. Crystallization and High-Temperature Structural Stability of Titanium Oxide Nanotube Arrays. *J. Mater. Res.* **2003**, *18*, 156–165. [[CrossRef](#)]
35. Hamlekhan, A.; Butt, A.; Patel, S.; Royhman, D.; Takoudis, C.; Sukotjo, C.; Mathew, M.T.; Shokuhfar, T. Optimization of Anodization and Annealing Condition Enhances TiO₂ Nanotubular Surface Hydrophilicity. In *TMS 2014: 143rd Annual Meeting & Exhibition*; Springer: Cham, Germany, 2014; pp. 221–228. [[CrossRef](#)]
36. Gulati, K.; Santos, A.; Findlay, D.; Losic, D. Optimizing Anodization Conditions for the Growth of Titania Nanotubes on Curved Surfaces. *J. Phys. Chem. C* **2015**, *119*, 16033–16045. [[CrossRef](#)]
37. Nogueira, R.P.; Uchoa, J.D.; Hilario, F.; Santana-Melo, G.D.F.; de Vasconcellos, L.M.R.; Marciano, F.R.; Roche, V.; Junior, A.M.J.; Lobo, A.O. Characterization of Optimized TiO₂ Nanotubes Morphology for Medical Implants: Biological Activity and Corrosion Resistance. *Int. J. Nanomed.* **2021**, *16*, 667–682. [[CrossRef](#)]
38. Zhang, H.; Banfield, J.F. Phase Transformation of Nanocrystalline Anatase-to-Rutile via Combined Interface and Surface Nucleation. *J. Mater. Res.* **2011**, *15*, 437–448. [[CrossRef](#)]
39. Gouma, P.I.; Mills, M.J. Anatase-to-Rutile Transformation in Titania Powders. *J. Am. Ceram. Soc.* **2001**, *84*, 619–622. [[CrossRef](#)]
40. Liu, H.Y.; Hsu, Y.L.; Su, H.Y.; Huang, R.C.; Hou, F.Y.; Tu, G.C.; Liu, W.H. A Comparative Study of Amorphous, Anatase, Rutile, and Mixed Phase TiO₂ Films by Mist Chemical Vapor Deposition and Ultraviolet Photodetectors Applications. *IEEE Sens. J.* **2018**, *18*, 4022–4029. [[CrossRef](#)]
41. Siah, W.R.; Lintang, H.O.; Shamsuddin, M.; Yuliati, L. High Photocatalytic Activity of Mixed Anatase-Rutile Phases on Commercial TiO₂ Nanoparticles. In *IOP Conference Series: Materials Science and Engineering, 10th Joint Conference on Chemistry 8–9 September 2015, Solo, Indonesia*; IOP Publishing: Bristol, UK, 2016; Volume 107, p. 012005. [[CrossRef](#)]
42. Fu, W.; Li, G.; Wang, Y.; Zeng, S.; Yan, Z.; Wang, J.; Xin, S.; Zhang, L.; Wu, S.; Zhang, Z. Facile Formation of Mesoporous Structured Mixed-Phase (Anatase/Rutile) TiO₂ with Enhanced Visible Light Photocatalytic Activity. *Chem. Commun.* **2017**, *54*, 58–61. [[CrossRef](#)] [[PubMed](#)]
43. Luo, Z.; Poyraz, A.S.; Kuo, C.H.; Miao, R.; Meng, Y.; Chen, S.Y.; Jiang, T.; Wenos, C.; Suib, S.L. Crystalline Mixed Phase (Anatase/Rutile) Mesoporous Titanium Dioxides for Visible Light Photocatalytic Activity. *Chem. Mater.* **2015**, *27*, 6–17. [[CrossRef](#)]
44. Rambabu, Y.; Jaiswal, M.; Roy, S.C. Effect of Annealing Temperature on the Phase Transition, Structural Stability and Photo-Electrochemical Performance of TiO₂ Multi-Leg Nanotubes. *Catal. Today* **2016**, *278*, 255–261. [[CrossRef](#)]

45. Zlamal, M.; Macak, J.M.; Schmuki, P.; Krýsa, J. Electrochemically Assisted Photocatalysis on Self-Organized TiO₂ Nanotubes. *Electrochem. Commun.* **2007**, *9*, 2822–2826. [[CrossRef](#)]
46. Brunauer, S.; Emmett, P.H.; Teller, E. Adsorption of Gases in Multimolecular Layers. *J. Am. Chem. Soc.* **2002**, *60*, 309–319. [[CrossRef](#)]
47. Suhadolnik, L.; Marinko, Ž.; Ponikvar-Svet, M.; Tavčar, G.; Kovač, J.; Čeh, M. Influence of Anodization-Electrolyte Aging on the Photocatalytic Activity of TiO₂ Nanotube Arrays. *J. Phys. Chem. C* **2020**, *124*, 4073–4080. [[CrossRef](#)]
48. Thirunavukkarasu, G.K.; Gowrisankaran, S.; Caplovicova, M.; Satrapinsky, L.; Gregor, M.; Lavrikova, A.; Gregus, J.; Halko, R.; Plesch, G.; Motola, M.; et al. Contribution of Photocatalytic and Fenton-Based Processes in Nanotwin Structured Anodic TiO₂ Nanotube Layers Modified by Ce and V. *Dalt. Trans.* **2022**. [[CrossRef](#)]
49. Arfanis, M.K.; Adamou, P.; Moustakas, N.G.; Triantis, T.M.; Kontos, A.G.; Falaras, P. Photocatalytic Degradation of Salicylic Acid and Caffeine Emerging Contaminants Using Titania Nanotubes. *Chem. Eng. J.* **2017**, *310*, 525–536. [[CrossRef](#)]
50. Marinko, Ž.; Suhadolnik, L.; Šetina Batič, B.; Šelih, V.S.; Majaron, B.; Kovač, J.; Čeh, M. Toward a Flexible and Efficient TiO₂ Photocatalyst Immobilized on a Titanium Foil. *ACS Omega* **2021**, *6*, 23233–23242. [[CrossRef](#)]